# Sensing analysis based on plasmon induced transparency in nanocavity-coupled waveguide

**Shiping Zhan, Hongjian Li,* Zhihui He, Boxun Li, Zhiquan Chen, and Hui Xu**

*College of Physics and Electronics, Central South University, Changsha 410083, China*
** lihj398@126.com*

**Abstract:** We report the sensing characteristic based on plasmon induced transparency in nanocavity-coupled metal-dielectric-metal waveguide analytically and numerically. A simple model for the sensing nature is first presented by the coupled mode theory. We show that the coupling strength and the resonance detuning play important roles in optimizing the sensing performance and the detection limit of sensor, and an interesting double-peak sensing is also obtained in such plasmonic sensor. In addition, the specific refractive index width of the dielectric environment is discovered in slow-light sensing and the relevant sensitivity can be enhanced. The proposed model and findings provide guidance for fundamental research of the integrated plasmonic nanosensor applications and designs.



**OCIS codes:** (250.5403) Plasmonics; (130.3120) Integrated optics devices; (280.4788) Optical sensing and sensors.

## References and links

1. D. Gramotnev and S. Bozhevolnyi, "Plasmonics beyond the diffraction limit," Nat. Photonics **4**(2), 83–91 (2010).
2. J. Yang, J. Lee, J. Kang, S. J. Oh, H. J. Ko, J. H. Son, K. Lee, J. S. Suh, Y. M. Huh, and S. Haam, "Smart drug-loaded polymer gold nanoshells for systemic and localized therapy of human epithelial cancer," Adv. Mater. **21**(43), 4339–4342 (2009).
3. I. Zand, M. Abrishamian, and T. Pakizeh, "Nanoplasmonic loaded slot cavities for wavelength filtering and demultiplexing," IEEE J. Sel. Top. Quantum Electron. **19**(3), 4600505 (2013).
4. H. A. Atwater and A. Polman, "Plasmonics for improved photovoltaic devices," Nat. Mater. **9**(3), 205–213 (2010).
5. S. Roh, T. Chung, and B. Lee, "Overview of the characteristics of micro- and nano-structured surface plasmon resonance sensors," Sensors **11**(2), 1565–1588 (2011).
6. N. Liu, M. Mesch, T. Weiss, M. Hentschel, and H. Giessen, "Infrared perfect absorber and its application as plasmonic sensor," Nano Lett. **10**(7), 2342–2348 (2010).
7. N. Liu, T. Weiss, M. Mesch, L. Langguth, U. Eigenthaler, M. Hirscher, C. Sönnichsen, and H. Giessen, "Planar metamaterial analogue of Electromagnetically Induced Transparency for plasmonic sensing," Nano Lett. **10**(4), 1103–1107 (2010).
8. R. Ameling, L. Langguth, M. Hentschel, M. Mesch, P. Braun, and H. Giessen, "Cavity-enhanced localized plasmon resonance sensing," Appl. Phys. Lett. **97**(25), 253116 (2010).
9. Q. Liu, J. S. Kee, and M. K. Park, "A refractive index sensor design based on grating-assisted coupling between a strip waveguide and a slot waveguide," Opt. Express **21**(5), 5897–5909 (2013).
10. J. Chen, Z. Li, S. Yue, J. Xiao, and Q. Gong, "Plasmon-Induced transparency in asymmetric T-shape single slit," Nano Lett. **12**(5), 2494–2498 (2012).
11. S. Zhan, H. Li, G. Cao, Z. He, B. Li, and H. Yang, "Slow light based on plasmon-induced transparency in dual-ring resonator-coupled MDM waveguide system," J. Phys. D Appl. Phys. **47**(20), 205101 (2014).
12. H. Wen, M. Terrel, S. Fan, and M. Digonnet, "Sensing with slow light in fiber Bragg gratings," IEEE Sens. J. **12**(1), 156–163 (2012).
13. H. Lu, X. Liu, D. Mao, and G. Wang, "Plasmonic nanosensor based on Fano resonance in waveguide-coupled resonators," Opt. Lett. **37**(18), 3780–3782 (2012).
14. J. Qi, Z. Chen, J. Chen, Y. Li, W. Qiang, J. Xu, and Q. Sun, "Independently tunable double Fano resonances in asymmetric MIM waveguide structure," Opt. Express **22**(12), 14688–14695 (2014).
15. G. Cao, H. Li, S. Zhan, H. Xu, Z. Liu, Z. He, and Y. Wang, "Formation and evolution mechanisms of plasmon-induced transparency in MDM waveguide with two stub resonators," Opt. Express **21**(8), 9198–9205 (2013).
16. Z. Han and S. I. Bozhevolnyi, "Plasmon-induced transparency with detuned ultracompact Fabry-Perot resonators in integrated plasmonic devices," Opt. Express **19**(4), 3251–3257 (2011).

#241662 Received 25 May 2015; revised 9 Jul 2015; accepted 23 Jul 2015; published 27 Jul 2015

17. Z. He, H. Li, S. Zhan, G. Cao, and B. Li, “Combined theoretical analysis for plasmon-induced transparency in waveguide systems,” Opt. Lett. **39**(19), 5543–5546 (2014).
18. Y. Huang, C. Min, and G. Veronis, “Subwavelength slow-light waveguides based on a plasmonic analogue of electromagnetically induced transparency,” Appl. Phys. Lett. **99**(14), 143117 (2011).
19. Y. Huang, C. Min, P. Dastmalchi, and G. Veronis, “Slow-light enhanced subwavelength plasmonic waveguide refractive index sensors,” Opt. Express **23**(11), 14922–14936 (2015).
20. J. Gu, R. Singh, X. Liu, X. Zhang, Y. Ma, S. Zhang, S. A. Maier, Z. Tian, A. K. Azad, H. T. Chen, A. J. Taylor, J. Han, and W. Zhang, “Active control of electromagnetically induced transparency analogue in terahertz metamaterials,” Nat. Commun. **3**, 1151 (2012).
21. Z. Han, E. Forsberg, and S. He, “Surface plasmon Bragg gratings formed in Metal-Insulator-Metal waveguides,” IEEE Photonics Technol. Lett. **19**(2), 91–93 (2007).
22. Q. Li, T. Wang, Y. Su, M. Yan, and M. Qiu, “Coupled mode theory analysis of mode-splitting in coupled cavity system,” Opt. Express **18**(8), 8367–8382 (2010).
23. A. Taflove and S. Hagness, Computational Electrodynamics: *The Finite-Difference Time-Domain Method, 3rd ed*, Artech, House, Boston, (2005).
24. P. Berini, “Bulk and surface sensitivities of surface plasmon waveguides,” New J. Phys. **10**(10), 105010 (2008).
25. W. C. Lai, S. Chakravarty, Y. Zou, Y. Guo, and R. T. Chen, “Slow light enhanced sensitivity of resonance modes in photonic crystal biosensors,” Appl. Phys. Lett. **102**(4), 041111 (2013).
26. T. Krauss, “Slow light in photonic crystal waveguides,” J. Phys. D Appl. Phys. **40**(9), 2666–2670 (2007).
27. G. Cao, H. Li, S. Zhan, Z. He, Z. Guo, X. Xu, and H. Yang, “Uniform theoretical description of plasmon-induced transparency in plasmonic stub waveguide,” Opt. Lett. **39**(2), 216–219 (2014).
28. M. Povinelli, S. Johnson, and J. Joannopoulos, “Slow-light, band-edge waveguides for tunable time delays,” Opt. Express **13**(18), 7145–7159 (2005).

## 1. Introduction

The extraordinary property of surface plasmon polaritons (SPPs), manipulating light on nanoscale structure beyond the diffraction limit [1], provides opportunities for many fascinating researches like biomedicine [2], optical filter [3], solar cell [4] and plasmonic sensor [5]. As a promising application, the plasmonic sensors based on varied systems have attracted people’s attention in the recent years [6–9]. Previous works showed the plasmon induced transparency (PIT) based sensor can be fabricated in metamaterial [7], and the PIT sensor performs better than the non-PIT one due to the steeper variation in the optical spectrum [10]. In addition, the PIT system possesses slow-light that can enhance the light-matter interaction, which can be used in sensors and slow-light devices [11, 12].

Lately, the nanoresonator-coupled metal-dielectric-metal (NCMDM) waveguide structure, with advantages of easy fabrication, light manipulation and convenient integration, has also been found available for the sensor research [13–15]. Lu et al reported a plasmonic sensor in a waveguide system and got a figure of merit (FOM) of ~500 [13], and Qi et al also observed a sensing phenomenon in the MDM waveguide structure and achieved FOMs over 650 [14]. Nevertheless, these researches mainly focused on the sensors’ performance numerically, the further sensing optimization based on analytical model is seldom discussed. In addition, many reports revealed that the PIT effect can also be realized in NCMDM waveguide systems [15–18]. From the above discussion, we think that the PIT waveguide system is an ideal candidate for the integrated plasmonic sensor. Very recently, Huang et al reported a PIT-based sensor in a MDM waveguide system and found the sensing performance can be enhanced [19]. However, more efforts still need to be made in the analytical and numerical research on the PIT-based sensor and its tuning mechanism in NCMDM waveguide system.

In this paper, a simple PIT-based nanosensor is proposed and an analytical expression of figure of merit is derived for the first time to our knowledge to characterize the sensing property. The coupling strength and the resonance detuning between the cavities are useful for the sensing tuning and optimization. And an interesting double-peak sensing is obtained by choosing the detuning in a certain range. Finally, the slow-light sensing of the PIT-based sensor is discussed and the relevant sensitivity can also be regulated.

#241662 Received 25 May 2015; revised 9 Jul 2015; accepted 23 Jul 2015; published 27 Jul 2015
 

## 2. Structure and analytical expression

The plasmonic nanosensor and its equivalent model are shown in Fig. 1. Two cavities with length $L_1$ (cavity 1), $L_2$ (cavity 2) and width $w$ are placed above the bus waveguide. The coupling distances are $h$ and $s$, respectively. When the incident pulse comes into the waveguide, SPP wave generates in both metal-dielectric interfaces. According to the evanescent coupling, two excitation pathways interfere destructively and result in an EIT-like spectrum. Cavity 1 and 2 can also be analogically regarded as the subradiant and the superradiant mode, respectively [20]. The permittivity of the dielectric environment during the sensing process is $\varepsilon_d$. And the metal is silver, with permittivity $\varepsilon_m$ defined by the Drude model [21]: $\varepsilon_m(\omega) = \varepsilon_\infty - \omega_p/(\omega^2 + i\omega\gamma_p)$, where $\omega$ stands for the angle frequency of the incident wave, $\varepsilon_\infty = 3.7$, $\omega_p = 1.38 \times 10^{16}$ rad/s is the bulk plasmon frequency, and $\gamma_p = 2.73 \times 10^{13}$ rad/s stands for the damping rate.

Based on coupled mode theory analysis [22], the stable state of cavity 2 can be described by a harmonic oscillator model as follows

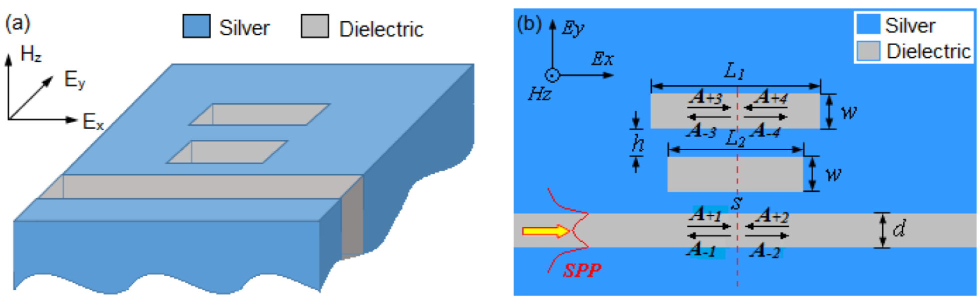


**Fig. 1.** The (a)schematic and (b)top view of the 2D plasmonic sensor in NCMDM waveguide system.

$$i\omega a = (i\omega_0 - 1/\tau_i - 1/\tau_w - 1/\tau_c)a + A_{+1}\sqrt{1/\tau_w} + A_{+3}\sqrt{1/\tau_c} + A_{+4}\sqrt{1/\tau_c}. \tag{1}$$

Here $a$ represents the mode amplitude of cavity 2, $\omega$ $(\lambda)$ is the angular frequency (wavelength) of the input optical pulse, $\omega_0$ is the resonant frequency, $1/\tau_i = \omega_0/(2Q_i)$ is the internal loss, $1/\tau_w = \omega_0/(2Q_w)$ and $1/\tau_c = \omega_0/(2Q_c)$ are the coupling loss to the waveguide and cavity 1, respectively. $Q_i$, $Q_w$, $Q_c$ are the related quality factors. The energy amplitudes in the bus waveguide and cavity 1 are depicted by $A_{\pm j}$ ($j$ = 1, 2, 3, 4). And they also satisfy the following relations

$$A_{-2} = A_{+1} - \sqrt{1/\tau_w}a,\ A_{-3} = A_{+4} - \sqrt{1/\tau_c}a,\ A_{-4} = A_{+3} - \sqrt{1/\tau_c}a, \tag{2}$$

$$A_{+3} = A_{-3}C\exp(-i\varphi),\ A_{+4} = A_{-4}C\exp(-i\varphi), \tag{3}$$

where $\varphi = 2\pi\mathrm{Re}(n_{eff})L_1/\lambda + \psi$ represents the phase shift for a half roundtrip in cavity 1, $C$ is the related attenuation coefficient, and $\psi$ is the additional phase shift by end-reflection in cavity 1. The effective refractive index $n_{eff}$ in a MDM waveguide with width $w$ can be obtained in [16].Thus the transmission coefficient at frequency $\omega$ of the entire system with dielectric refractive index $n$, where $n = (\varepsilon_d)^{1/2}$, is derived as

$$T(\omega,n) = \left|A_{-2}/A_{+1}\right|^2 = \left|1 - \omega_0/(2KQ_w + \omega_0)\right|^2, \tag{4a}$$

where

$$K(\omega,n) = i(\omega - \omega_0) + \omega_0/2Q_i + \omega_0(1 - \mathrm{C}e^{i\varphi})\Big/\left[2Q_c(1 + \mathrm{C}e^{i\varphi})\right]. \tag{4b}$$

#241662 Received 25 May 2015; revised 9 Jul 2015; accepted 23 Jul 2015; published 27 Jul 2015

For numerical understanding of Eq. (4), the FDTD simulation with grid size $\Delta x = \Delta y = 2.5$nm is provided for structure with $w = d = 50$nm, $s = 20$nm, $h = 40$nm, $L_1 = 415$nm and $L_2 = 400$nm [23]. In Fig. 2(a), a typical EIT-like feature (blue cycles) is observed, where a transparency peak at 674nm is located between two dips at 650nm and 691.6nm [10]. That is consistent with the analytical one (red solid lines) based on Eq. (4).

Thus, the transmission at frequency $\omega$ for the system with dielectric material refractive index $n + \Delta n$ can be derived as

$$T(\omega, n+\Delta n) = \left| 1 - \frac{\omega_1 / 2Q_w'}{i(\omega - \omega_1) + \omega_1 / 2Q_i' + \omega_1 / 2Q_w' + (\omega_1 / 2Q_c)(1 - \mathrm{C}e^{i\varphi'})/(1 + \mathrm{C}e^{i\varphi'})} \right|^2, \quad (5)$$

where $\omega_1 = \omega_0/(n + \Delta n)$, $Q_i'$ and $Q_w'$ are the resonance frequency and quality factors when the environment refractive index increases from $n$ to $n + \Delta n$, while $\varphi'$ is the half roundtrip phase shift in cavity 1. It's worthy to notice that those values are obtained due to the approximation that the line shape of the optical response spectrum nearly maintains the same, only leading to a red-shift [13, 14], and it's also been proved by the later analysis.

Based on the definition of figure of merit [8] and the consideration that detection used in sensor, such as biosensor, usually by measuring the light intensity variation for one particular wavelength, here we give a precise analytical expression for FOM at frequency $\omega$ as

$$\boxed{FOM(\omega) = \frac{\Delta T}{T\Delta n} = \frac{T(\omega, n+\Delta n) - T(\omega, n)}{T(\omega, n)\Delta n},} \quad (6)$$

where $T(\omega,n)$ and $T(\omega,n + \Delta n)$ have been obtained in Eq. (4) and (5), $\Delta T$ is the intensity variation at frequency $\omega$ caused by environment refractive index change $\Delta n$. The simulated sensing response for the PIT-based sensor in Fig. 2(a) is shown in Fig. 2(b). The spectrum

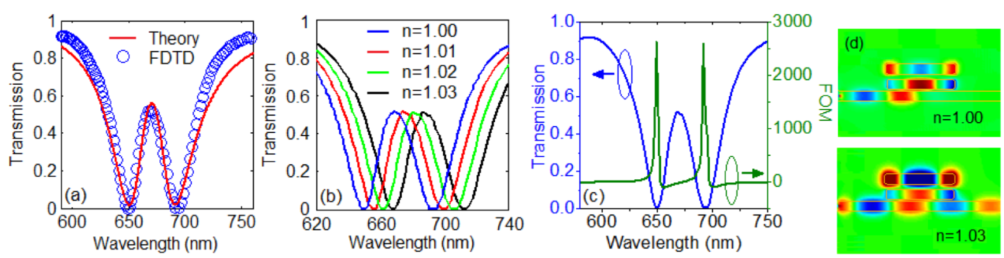


Fig. 2. (a) Simulated transmission (blue cycles) and theoretical fitting (red solid lines) as $\omega_0 = 2.81 \times 10^{15}$rad/s, $Q_c = 100$, $Q_w = 10$, $Q_i = 339$, $C = 0.95$, $\psi = 4.81$rad. (b) Transmission for with varied $n$. (c) Transmission and FOM as functions of wavelength. (d) Magnetic field distributions of incident pulse at 691.6nm for $n = 1.00$ and $n = 1.03$.

shifts to longer wavelength and almost keeps the line-shape. A FOM of ~2600 at 691.6nm is obtained, which is much higher than that in [13, 14], here $\Delta n$ is chosen to be 0.01. Figure 2(c) shows the transmission and FOM as functions of wavelength. The maximum FOM nearly appears at the transmission dips, which can be explained by the lowest initial intensity $T$ here. The magnetic field distribution of the incident pulse at 691.6nm with $n = 1.00$ and 1.03 are displayed in Fig. 2(d). As the surrounding refractive index increases, the plasmonic sensor also shows a switching property.

### 3. Numerical results

To verify the availability of the analytical sensing expression in Eq. (6), we first focus on the coupling strength between the two cavities, which is represented by $Q_c$. Figure 3(a) is the theoretical evolution of FOM with $Q_c$, here we take $\Delta n = 0.01$ and the structure parameters used in Fig. 2(a). It can be observed that the FOM maximum for the left dip (dip 1) increases

#241662 Received 25 May 2015; revised 9 Jul 2015; accepted 23 Jul 2015; published 27 Jul 2015
 

gradually while decreases for the right one (dip 2) when $Q_c$ gets enlarged, and a highest value reaches almost 820. This is because the lower coupling strength makes the closer transmission dips, thus the $\Delta T$s caused by $\Delta n$ for the two dips vary differently, which relult in this phenomenon. Numerical analysis obtianed by FDTD method is provided to support this explanation. The simulated intensity variations at dips caused by $\Delta n = 0.01$ for different coupling distance $h$ are shown in Fig. 3(b). When $h$ changes from 32 to 64nm, indicating the enlarged $Q_c$, the $\Delta T$ increases for dip 1 (black squares) while decreases for the second (red circles). Since the dip transmissions are quite small, we make them constant values approximately, which leads to the proportional relationship between FOM and $\Delta T$. Thus, as $Q_c$ increases, the opposite variation of $\Delta T$ leads to the different trend of FOM, which agrees with the theoretical results in Fig. 3(a). For further understanding the impact of the coupling strength, we discuss the lossless situation of subradiant cavity for $C = 1$, shown in Fig. 3(c). Different from Fig. 3(a), the FOM in lossless case almost maintains the same for the first dip but shows an nonmonotonic change for the second one when $Q_c$ increases. We find lowering the attenuation in the subradiant resonator can also adjust the sensing property. Figure 3(d)-(f) are the transmission spectra for varied coupling strength. It is found that the transmission change $\Delta T$ for the right dip firstly increases from 0.165 to 0.374 but then drops to 0.206, thus the related FOM behaves a nonmonotonic variation according to the former discussion. In addition, we know for realistic sensor device, there should be a detection limit [24]. That means when the sensing is under certain condition, the plasmonic sensor can show good performance. But if the sensing work is beyond that condition, the sensor will lose efficacy. Such as when $T$ is quite small, the sensor may not be able to detect small refractive index change, which leads to a detection limit. Here we use the definition of detection limit in Ref [24]. as:$\Delta n_{lim} = (\Delta n/\Delta T)\Delta T_{lim}$, where $\Delta n_{lim}$ represents the smallest refractive index change of the tested material or analyte, $\Delta T$ and $\Delta n$ have been defined above, while $\Delta T_{lim}$ is the minimum transmission change that can be detected, which is determined by the optical detector. We also define a modified figure of merit as $\mathrm{FOM_m} = \Delta T/\Delta n$ accordingly. Can the structure parameter also affect the detection limit of the PIT-based sensor? Now we discuss this issue. For sensing analysis of dip 1, the detection limit $\Delta n_{lim}$ and $\mathrm{FOM_m}$ as functions of the coupling distance $h$ are shown in Fig. 3(g). A tradeoff is found between the $\Delta n_{lim}$ and the $\mathrm{FOM_m}$ due to the fact that the detection limit $\Delta n_{lim}$ is inversely proportional to $\Delta T/\Delta n$. The $\Delta n_{lim}$ decreases while the $\mathrm{FOM_m}$ increases as the coupling gets weak. A highest $\Delta n_{lim}$ of ~$0.137\Delta T_{lim}$ is obtained under strong coupling with $h = 32$nm, while the $\mathrm{FOM_m}$ reaches its maximum of ~20 under weak coupling with $h = 64$nm. Since the $\Delta T_{lim}$ is usually a constant that determined by the optical detector, thus the coefficient in front of $\Delta T_{lim}$ can properly describe the detection limit of a plasmonic sensor. However, for dip 2, the highest $\Delta n_{lim}$ of ~$0.313\Delta T_{lim}$ is obtained under weak coupling with $h = 64$nm, while the $\mathrm{FOM_m}$ reaches its maximum of ~14 under strong coupling with $h = 32$nm, shown in Fig. 3(h), which is opposite to the results of dip 1. This can also be simply explained by the relationship between the intensity variations $\Delta T$ and the coupling distance $h$ in Fig. 3(b). These interesting findings can be helpful in optimizing the sensing property and the detection limit of PIT-based sensor by tuning the coupling strength between the superradiant and the subradiant cavities.

#241662 Received 25 May 2015; revised 9 Jul 2015; accepted 23 Jul 2015; published 27 Jul 2015

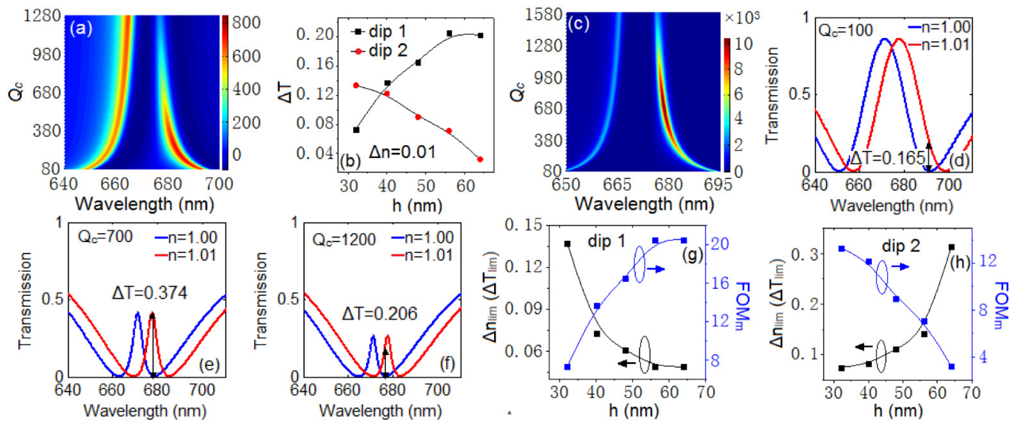


**Fig. 3.** The evolution of FOM with $Q_c$ for $\Delta n$ = 0.01in (a) lossy and (c)lossless system. (b) Intensity variation $\Delta T$ at dips caused by $\Delta n$ = 0.01 for different coupling distance $h$. (d)-(f) The transmission spectra for $n$ = 1.00 and 1.01 with $Q_c$ = 100, 700 and 1200, respectively. (g) and (h) are $\Delta n_{lim}$ and FOM$_{\mathrm{m}}$ as functions of coupling distance $h$.

Besides the coupling strength, the resonance detuning between the two cavities, tuned by length $L_1$, also can affect the sensing characteristic. Figure 4(a) is the FOM evolution with cavity length $L_1$.The white dash line represents $L_1$ = 415nm which guarantees the symmetric transmission spetrum. When $L_1$ gets larger (smaller) than 415nm, only one obvious left (right) sensing peak appears. Paticularly, when $L_1$ = 415nm, two comparable sensing peaks with FOM of nearly 700 are found. We name it as a double-peak (DP) sensing phenomenon. The double-peak sensing may perform more functionally than the conventional single-peak sensing. This interesting phenomenon was also found in [14]. Figure 4(b) is the simulated intensity variation $\Delta T$ caused by $\Delta n$ = 0.01 for different $L_1$. It can be seen that the difference between the two $\Delta T$s gets enlarged when $L_1$ becomes larger or smaller than 415nm. Thus there should be an operating width of $L_1$ that ensures the DP sensing. However, the attenuation of subradiant cavity makes such width quiet small, only about several nanometers. If the width can be broadened, it could be beneficial for the sensor fabrication and meanwhile lower the technique difficulty. Figure 4(c) shows the evolution of FOM with $L_1$ in the ideal situation ($C$ = 1) for different $Q_c$. For potential applications, high FOM is required, we choose the minimum of 500 in the color label for discussion. When $Q_c$ = 100, the DP sensing range is obseved from $L_1$ = 376 to 473nm, resulting in an operating width of 97nm. Here some outer part of Fig. 4(c) is not given for clarity. Similarly, the operating DP width for $Q_c$ = 200 and 400 are calculated as 66 and 43nm, respectively. It's found that the coupling strength can affect the width and a stronger coupling makes a wider operating range, however, a relatively lower FOM. Later on, we briefly discuss the influence of coefficient $C$, shown in Fig. 4(d). The lower attenuation results in the larger DP width. And the coupling strength can also be regarded as the further tuning factor. This can be helpful for the design and improvement of highly tunable sensor with multi-sensing application. In addition, similar with the discussion in Fig. 3(g)-3(h), the detection limit $\Delta n_{lim}$ and the FOM$_{\mathrm{m}}$ of the plasmonic sensor can also be regulated by the resonance detuning between superradiant and the subradiant cavities, shown in Fig. 4(e)-4(f). For sensing analysis of dip 1, the $\Delta n_{lim}$ increases while the FOM$_{\mathrm{m}}$ decreases as L1 gets weak. A highest $\Delta n_{lim}$ of ~0.2$\Delta T_{lim}$ is obtained when $L_1$ = 435nm, while the FOM$_{\mathrm{m}}$ reaches its maximum of ~24 for $L_1$ = 395nm. For dip 2, however, the highest $\Delta n_{lim}$ of ~0.294$\Delta T_{lim}$ is obtained for $L_1$ = 395nm, while the modified figure of merit gets a peak value of ~40. This can be simply explained by the Fano-shaped spectra that results from the resonance detuning between the superradiant and the subradiant modes [13]. These results can be useful in optimizing the sensing property and the detection limit by tuning the resonance detuning in PIT-based sensor.

#241662 Received 25 May 2015; revised 9 Jul 2015; accepted 23 Jul 2015; published 27 Jul 2015

Since the sensor is based on a PIT system, thus besides of the conventional sensing above, a slow-light sensing [12, 25] should also be realized. Attributing to the steep phase dispersion in transparency window, the group velocity of light can be slowed down significantly and results in a time delay. The decrease of group velocity allows not only the light to 'feel' changes in the refractive index for a longer time, but also the enhancement of light intensity by the pulse compression [26], give rise to good sensing performance. The group index $N_g$ can be calculated through $N_g = c/v_g = c/H{\cdot}\tau_g = c/H{\cdot}(d\theta(\omega)/d\omega)$ [27], where $v_g$ is the group velocity, $\tau_g$ is delay time, and the phase shift $\theta(\omega)$ is the function of angular frequency $\omega$, $H$ = 1000nm is the length of the plasmonic system. Figure 5 (a) is the group index for $Q_c$ = 600 and $L_1$ = 415nm with $n$ = 1.000, 1.005 and 1.012. When $n$ = 1.005, the pulse centered at 679nm has a group index of 2 as it passes through the system. This means the light speed is halved, and the group index (or intensity) of the pulse increases as $n$ increases, but reaches a maximum of ~22 when $n$ = 1.012. Here we consider $N_g \geq 2$ as slow-light region and define the sensing width with slow-light (SWS) as SWS = 1.012-1.005 = 0.007. The SWS reveals the available detection limit of a sensor for slow-light sensing. Figure 5(b) shows the SWS as a function of $L_1$ for different $Q_c$. It is found that both the resonance detuning and the coupling strength can adjust the SWS of palsmonic sensor. From $L_1$ = 400 to 415nm, the SWS decreases gradually and lower $Q_c$ leads to

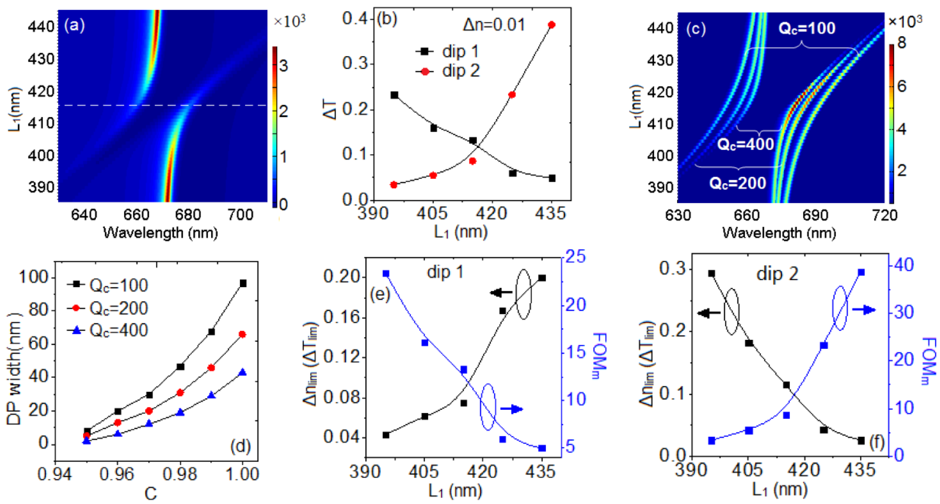


**Fig. 4.** The evolution of FOM (a) with $L_1$ in the lossy case of $C$ = 0.95, (b)The simulated transmission changre $\Delta T$ at two dips as a function of $L_1$. (c) The evolution of FOM with $L_1$ for different $Q_c$ in the lossless case of $C$ = 1, (d)The relationship between DP width and attenuation coefficient $C$ for different $Q_c$. (e) and (f) are $\Delta n_{lim}$ and $\mathrm{FOM_m}$ as functions of cavity length $L_1$.

larger quantity for each $L_1$. The difference at $L_1$ = 395nm may result from the large resonance detuning. For sensing application, higher SWS guarantees wider refractive index range of the dielectric environment or the tested analyte. Based on the figure of merit analysis by M. Povinelli [28], we further give the sensitivity of system with slow-light at frequency $\omega$ as $\mathrm{FOM}_{Ng}(\omega) = [N_g(\omega, n + \Delta n) - N_g(\omega, n)]n/(N_g(\omega, n)\Delta n)$, here $\Delta n$ is chosen to be the SWS. Figure 5(c) depicts the relationship between the sensing width and the $\mathrm{FOM}_{Ng}$ for structures with varied $L_1$ when $Q_c$ = 600. A tradeoff exists apparently and higher sensitivity makes smaller sensing width. The balance between these two factors can be interesting and will be discussed

#241662 Received 25 May 2015; revised 9 Jul 2015; accepted 23 Jul 2015; published 27 Jul 2015

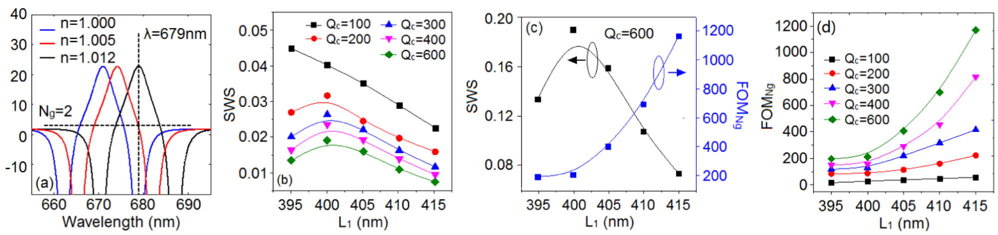

**Fig. 5.** (a) The group index for $Q_c$ = 600, $L_1$ = 415nm with different refractive index, (b) The SWS as a function of $L_1$ with different $Q_c$, (c) The relationship between the SWS and the $FOM_{Ng}$ for varied $L_1$ when $Q_c$ = 600. (d) $FOM_{Ng}$ for varied $L_1$ with different $Q_c$.

in the future. The detuning of resonance can also affect the SWS and the $FOM_{Ng}$, lower detuning results in a higher sensitivity and a maximum of ~1200 is achieved when $L_1$ = 415nm for the nearly zero detuning. The relation between $L_1$ and $FOM_{Ng}$ under varied coupling strength is displayed in Fig. 5(d). For each constant coupling strength, the $FOM_{Ng}$ increases as $L_1$ gets larger, but the slope strongly depends on the quality factor $Q_c$. This is because the SWS decreases while the maximum group index $N_g(\omega, n + \Delta n)$ increases when enlarging $L_1$, and the slow-light sensitivity is proportional to the $N_g(\omega, n + \Delta n)$ but inversely proportional to the SWS according to the definition. Moreover, the overall sensitivities for higher $Q_c$ are larger than those for smaller $Q_c$ which may be attributed to the steeper dispersion in transparency windows. According to the discussion above, the slow-light sensing in the PIT-based sensor is found enhanced by weak coupling and small detuning between the superradiant cavity and the subradiant cavity. These findings may provide help for the theoretical and application research of plasmonic nanosensor with slow-light.

## 4. Conclusions

In summary, the sensing property of PIT-based sensor in nanocavity-coupled MDM waveguide is investigated, and a simple analytical expression is presented for discussion. It is found that the sensing performance and the detection limit of our proposed sensor can be adjusted by the coupling strength, resonance detuning and dissipation, the double-peak sensing phenomenon can be observed within certain detuning. Finally, the refractive index range for the slow-light sensing is discussed and the related sensitivity is realized adjustable. This work may provide guidance for fundamental applications and designs of plasmonic nanosensor.

## Acknowledgments

This work was funded by the Fundamental Research Funds for the Central Universities of Central South University under Grant No. 72150050429 and the National Natural Science Foundation of China under Grant No. 61275174.